Planar isothermal solidification from an undercooled melt: Unsteady solute segregation studied with the phase-field model

M. Conti
Dipartimento di Matematica e Fisica, Universita' di Camerino, 62032 Camerino, Italy
(Received 10 June 1996)

The planar isothermal solidification of a binary alloy is studied through the phase-field model. The model includes gradient energy terms for both the phase and concentration fields. The long time attractor of the process was identified in a previous study by Wheeler, Boettinger, and McFadden [Phys. Rev. E **47**, 1893 (1993)] in the limit of vanishing small values of ϵ/δ, where ϵ and δ are the coefficients of the phase-field and concentration gradient energies, respectively. In that limit the main results of the continuous growth model (CGM) of Aziz and Kaplan [Acta Metall. **36**, 2335 (1988)] were substantially recovered. The present study is focused on the first transient of the process, when the solute profile is not yet fully developed. We found that in this stage the solute segregation at the solid-liquid interface deviates from the predictions of the CGM, as the solute partitioning is contrasted by the energy cost required to substain large concentration gradients. [S1063-651X(97)07901-4]

PACS number(s): 64.70.Dv, 68.10.Gw, 81.30.Bx, 82.65.Dp

I. INTRODUCTION

The understanding and prediction of the interfacial dynamics in rapid solidification of binary alloys is a matter of growing interest. The subject was addressed in several studies and through different perspectives.

Sharp interface models utilize the diffusion equation to describe the long range transport of solute [1,2]; the boundary conditions imposed at the solid-liquid interface reflect two different constraints: (i) the conservation of solute across the moving front, and (ii) a couple of constitutive laws that relate the composition of the growing solid and the front velocity v to the temperature T and to the interfacial melt composition. The latter conditions are derived through a separate modelization of the interface kinetics on a microscopic scale. Much effort has been devoted to this point. It is well known that in rapid solidification processes the partition coefficient k (the ratio of solute concentration c in the growing solid to that in the liquid at the interface) deviates from its equilibrium value k_e and increases towards unity at large growth rates. This phenomenon, termed ''solute trapping'' [3], was explained by Aziz and Kaplan [4] and Aziz and Boettinger [5] within the continuous growth model (CGM) as the result of a diffusive redistribution of the solute and the solvent across the moving front.

A different technique to investigate alloy solidification is based on the phase-field model (PFM). Within this approach a phase field $\phi(x,t)$ characterizes the phase of the system at each point. A free-energy (or entropy) functional is then constructed, that depends on ϕ as well as on the concentration and temperature fields. Gradient terms account for the energy cost associated to the solid-liquid interface. The extremization of the functional in respect to these variables results in the dynamic equations for the evolution of the process. A first PFM for solidification of binary solutions was developed by Wheeler, Boettinger, and McFadden (WBM1) [6] in the isothermal approximation. They started from a Landau-Ginzburg free energy functional depending on the bulk free energy density and including a $(\nabla\phi)^2$ term. In their study an asymptotic analysis was conducted to demonstrate that the model recovers the classical sharp interface formulation when the interfacial layer is sufficiently thin; moreover, the characteristic parameters of the PFM were related to the actual material properties. However, their model failed to describe properly the segregation of solute at the interface, as the partition coefficient resulted a decreasing function of the front velocity.

In a successive study Wheeler, Boettinger, and McFadden (WBM2) [7] identified the origin of this inconsistency, observing that an energy cost is associated not only to the gradients of the ϕ field, but to the gradients of concentration as well. To account for this effect, the new model they developed included a $(\nabla c)^2$ term, acting to oppose the contraction of the solute profile at large velocities. An asymptotic analysis was performed in the limit of steady growth and for $\epsilon/\delta \to 0$, where ϵ and δ are the coefficients of the phase-field and concentration gradient energies, respectively. Equal solute diffusivities were assumed in the solid and liquid phases. Within these limits the solute segregation at the moving interface was properly described, and the results of the CGM were substantially recovered.

However, rapid solidification of binary mixtures often involves melting and regrowth of thin films (10^{-5} cm) deposited onto a substrate as, for example, in pulsed-laser melting experiments [8]. In these conditions the steady regime could hardly be observable and the analysis of the growth process should be focused on its transient characteristics. This is the aim of the present study: the planar isothermal growth of a solid germ is numerically simulated and followed during the transient stage when the solute profile is not yet fully developed.

The time dependent equations of the phase-field model are derived starting from an entropy functional, along the lines suggested by Penrose and Fife [9] and successively followed by Wang *et al.* [10] and Warren and Boettinger [11]. The inclusion of the $(\nabla c)^2$ term makes the model formulation very similar to that given by WBM2. We allow for

different solute diffusivities in the solid and liquid phases, and the effect of the ratio ϵ/δ on the growth process is also analyzed. We found that in the transient stage the solute segregation at the solid-liquid interface deviates from the predictions of the CGM, as the solute partitioning is contrasted by the energy cost required to substain large c gradients.

The paper is organized as follows: in Sec. II the governing equations will be derived, starting from an entropy formulation of the model; the equations will be utilized to study the solidification of a nickel-copper ideal solution. In Sec. III some details of the numerical method will be given, and in Sec. IV the results of the numerical simulations will be presented. The conclusions will follow in Sec. V.

II. DEVELOPMENT OF THE MODEL

A. Derivation of the governing equations

The system is an initially undercooled binary alloy of components A (solvent) and B (solute). As a starting point we define an entropy functional as

$$\mathcal{S}=\int\left[s(e,\phi,c)-\frac{\epsilon^2}{2}\left|\nabla\phi\right|^2-\frac{\delta^2}{2}\left|\nabla c\right|^2\right]dv, \tag{1}$$

where integration is performed over the system volume; s is the thermodynamic entropy that depends on the internal energy density e and on the concentration and phase fields; the coefficients ϵ and δ account for the gradient term corrections. The phase field ϕ assumes the values $\phi=0$ in the solid and $\phi=1$ in the liquid; intermediate values correspond to the interface between the two phases. A conservation law governs the solute transport

$$\dot{c}=-\nabla\cdot\mathbf{J}_c. \tag{2}$$

To ensure that the local entropy production is always positive, the solute flux can be written in a simple form as

$$\mathbf{J}_c=M_c\nabla\frac{\delta\mathcal{S}}{\delta c}, \tag{3}$$

and the evolution of the phase field is given by

$$\dot{\phi}=M_\phi\frac{\delta\mathcal{S}}{\delta\phi}, \tag{4}$$

where M_c and M_ϕ are positive constants.

The variational derivatives in the above equations are given by

$$\frac{\delta\mathcal{S}}{\delta c}=\frac{\partial s}{\partial c}+\delta^2\nabla^2 c=\frac{\mu^A-\mu^B}{T}+\delta^2\nabla^2 c, \tag{5}$$

$$\frac{\delta\mathcal{S}}{\delta\phi}=\frac{\partial s}{\partial\phi}+\epsilon^2\nabla^2\phi. \tag{6}$$

In Eq. (5) μ^A and μ^B are the chemical potentials of the solvent and the solute, given for an ideal solution, respectively, by

$$\mu^A=f^A(\phi,T)+\frac{RT}{v_m}\ln(1-c), \tag{7}$$

$$\mu^B=f^B(\phi,T)+\frac{RT}{v_m}\ln(c). \tag{8}$$

Here R is the gas constant and v_m is the molar volume; f^A and f^B are the free-energy densities of the pure species A and B. To evaluate f^A, the internal energy density of pure A is postulated of the form

$$e^A(T)=e_s^A(T)+p(\phi)[e_l^A(T)-e_s^A(T)], \tag{9}$$

where e_s^A and e_l^A are the internal energy densities in the solid and in the liquid phases, respectively; the function $p(\phi)$ is monotonically increasing from $p(0)=0$ in the solid to $p(1)=1$ in the liquid. Assuming constant and equal values for the specific heat C^A in both phases, the energy densities e_s^A and e_l^A can be written as

$$e_s^A(t)=e_s^A(T_m^A)+C^A(T-T_m^A), \tag{10}$$

$$e_l^A(T)=e_l^A(T_m^A)+C^A(T-T_m^A), \tag{11}$$

where T_m^A is the melting temperature of pure A.

The difference

$$L^A=e_l^A(T_m^A)-e_s^A(T_m^A) \tag{12}$$

gives the latent heat per unit volume of species A. Then $f^A(\phi,T)$ can be written as

$$f^A=TG^A(\phi)+[e_s^A(T_m^A)-C^AT_m^A+p(\phi)L^A]\left(1-\frac{T}{T_m^A}\right)-C^AT\ln\left(\frac{T}{T_m^A}\right). \tag{13}$$

In Eq. (13) the function $G^A(\phi)$ is given by

$$G^A(\phi)=\tfrac{1}{4}W^A\phi^2(1-\phi)^2, \tag{14}$$

that is, a symmetric double well potential with equal minima at $\phi=0$ and $\phi=1$, scaled by the positive well height W^A.

Choosing the function $p(\phi)$ as $p(\phi)=\phi^3(10-15\phi+6\phi^2)$ the condition is enforced that bulk solid and liquid are described by $\phi=0$ and $\phi=1$, respectively, for every value of temperature. Equation (13) still holds for the free energy f^B if all the material parameters, labeled with the superscript A are replaced with the ones related to the B species.

Now the free energy of the solution is introduced as

$$f=(1-c)\mu^A+c\mu^B \tag{15}$$

and use is made of the thermodynamic equation

$$\frac{\partial s}{\partial\phi}=-\frac{1}{T}\frac{\partial f}{\partial\phi}. \tag{16}$$

Then Eqs. (4), (6)–(8), (13), (15), and (16) yield the dynamic evolution of the phase field as

$$\frac{\partial \phi}{\partial t} = M_\phi[\epsilon^2 \nabla^2 \phi - (1-c) H^A(\phi,T) - c H^B(\phi,T)], \quad (17)$$

where the function $H^A(\phi,T)$ is defined as

$$H^A(\phi,T) = G'(\phi) - p'(\phi) L^A \frac{T - T_m^A}{T T_m^A} \quad (18)$$

and a similar expression holds for $H^B(\phi,T)$.

Starting from Eqs. (2), (3), and (5) and observing that

$$\nabla \frac{\mu^A - \mu^B}{T} = \frac{\partial}{\partial \phi} \frac{\mu^A - \mu^B}{T} \nabla \phi + \frac{\partial}{\partial c} \frac{\mu^A - \mu^B}{T} \nabla c, \quad (19)$$

where

$$\frac{\partial}{\partial \phi} \frac{\mu^A - \mu^B}{T} = H^A(\phi,T) - H^B(\phi,T), \quad (20)$$

$$\frac{\partial}{\partial c} \frac{\mu^A - \mu^B}{T} = -\frac{R}{v_m} \frac{1}{c(1-c)} \quad (21)$$

the dynamic equation for the concentration field is written as

$$\frac{\partial c}{\partial t} = -\nabla \cdot \left\{ D_c c(1-c) \frac{v_m}{R} \nabla(\delta^2 \nabla^2 c) + D_c c(1-c) \frac{v_m}{R} \times [H^A(\phi,T) - H^B(\phi,T)] \nabla \phi - D_c \nabla c \right\}. \quad (22)$$

In Eq. (22) the standard definition of the solute diffusivity D_c has been recovered taking

$$D_c = \frac{M_c}{c(1-c)} \frac{R}{v_m}. \quad (23)$$

Here and in the following the approximation is made $C^A = C^B = C$. The model is then synthetized through Eqs. (17) and (22). As the solute diffusivity is quite different in the solid and liquid phases, in the following D_c will be taken as

$$D_c = D_s + p(\phi)(D_l - D_s), \quad (24)$$

D_l and D_s being the diffusivities in the liquid and in the solid, respectively.

B. The nondimensional equations

A nondimensional version of the model is obtained scaling lengths to some reference scale ξ, and time to ξ^2/D_l; the nondimensional temperature is defined as $u = C(T - T_m^A)/L^A$ and the function $H^{A,B}(\phi,T)$ is scaled as $\tilde{H}^{A,B}(\phi,T) = (v_m/R) H^{A,B}(\phi,T)$.

We allow M_ϕ to depend on the local composition as

$$M_\phi = (1-c) M_\phi^A + c M_\phi^B \quad (25)$$

and we define the following nondimensional parameters:

$$\begin{gathered} \tilde{L} = \frac{L^B}{L^A} \quad \tilde{\epsilon}^{A,B} = \frac{\epsilon}{\xi \sqrt{W^{A,B}}} \\ n = \frac{M_\phi^A}{M_\phi^B} \quad u^* = \frac{C(T_m^A - T_m^B)}{L^A} \\ m = \frac{M_\phi^B \epsilon^2}{D_l} \quad E = \frac{v_m}{R} \frac{\delta^2}{\xi^2} \\ \tilde{W}^{A,B} = \frac{v_m}{R} W^{A,B} \quad \alpha^{A,B} = \frac{L^{A,B}}{CT} \frac{L^{A,B}}{T_m^{A,B}} \frac{\xi^2}{\epsilon^2} \tilde{\epsilon}^{A,B}. \end{gathered} \quad (26)$$

Then the nondimensional equations of the model become

$$\begin{aligned} \frac{\partial \phi}{\partial t} &= [(1-c)n + c] m \nabla^2 \phi - [(1-c)n + c] m \\ &\times \left\{ (1-c) \left[\frac{G'(\phi)}{\tilde{\epsilon}^{A2}} - \frac{p'(\phi) \alpha^A u}{\tilde{\epsilon}^A} \right] \right. \\ &\left. + c \left[\frac{G'(\phi)}{\tilde{\epsilon}^{B2}} - \frac{p'(\phi) \alpha^B (u + u^*)}{\tilde{\epsilon}^B \tilde{L}} \right] \right\}, \end{aligned} \quad (27)$$

$$\begin{aligned} \frac{\partial c}{\partial t} &= \nabla \cdot \{ \lambda(\phi) \nabla c - c(1-c) \lambda(\phi) \nabla (E \nabla^2 c) - c(1-c) \lambda(\phi) \\ &\times [\tilde{H}^A(\phi,T) - \tilde{H}^B(\phi,T)] \nabla \phi \}, \end{aligned} \quad (28)$$

where, in Eq. (28) $\lambda(\phi)$ is defined as

$$\lambda(\phi) = \frac{D_s}{D_l} + p(\phi) \left(1 - \frac{D_s}{D_l} \right). \quad (29)$$

C. Numerical values of the parameters

The model parameters $\alpha^{A,B}, \tilde{\epsilon}^{A,B}, \tilde{W}^{A,B}, m, n$ can be associated to the physical properties of the alloy components analyzing the planar solution of the phase-field equations for both isothermal steady growth and isothermal coexistence of liquid and solid. Details of this derivation are given in [6] and [11]; below only the results are synthesized:

$$\begin{gathered} \alpha^{A,B} = \frac{L^{A,B}}{CT} \frac{\xi L^{A,B}}{6\sqrt{2}\sigma^{A,B}} \\ \tilde{\epsilon}^{A,B} = \frac{h^{A,B}}{\xi} \\ \tilde{W}^{A,B} = \frac{v_m}{R} \frac{12\sigma^{A,B}}{\sqrt{2} T_m^{A,B} h_{A,B}} \\ m = \frac{\beta^B \sigma^B T_m^B}{D_l L^B} \\ n = \frac{\beta^A \sigma^A T_m^A L^B}{\beta^B \sigma^B T_m^B L^A}, \end{gathered} \quad (30)$$

TABLE I. Material parameters for the Ni-Cu alloy.

	Nickel	Copper
T_m (K)	1728	1358
L (J/cm^3)	2350	1728
v_m (cm^3/mole)[a]	7.0	7.8
σ (J/cm^2)	3.7×10^{-5}	2.8×10^{-5}
β (cm/K s)[b]	160	198
D_l (cm^2/s)	10^{-5}	10^{-5}

[a]An average value of 7.4 will be taken.
[b]From the estimation of Willnecker, Herlach, Feuerbacher [12].

where $\sigma^{A,B}$ is the surface tension of pure A or B; $\beta^{A,B}$ is the kinetic undercooling coefficient, that relates the interface undercooling to the interface velocity through $v=\beta^{A,B}(T_m^{A,B}-T)$. In the phase-field model, for a pure substance, the interface thickness is a free and independent parameter, that has been indicated in Eq. (30) through $h^{A,B}$. As ϵ is not allowed to depend on concentration, Eqs. (26) and (30) force the condition

$$\frac{h^B}{h^A}=\frac{\sigma^A T_m^B}{\sigma^B T_m^A}. \tag{31}$$

The gradient concentration coefficient δ, following the suggestion of WBM2, will be chosen so that $\epsilon/\delta\ll1$.

Table I summarizes the values of the thermophysical properties of nickel (A) and copper (B) utilized to estimate the above parameters. The length scale was fixed at $\xi=2.1\times10^{-4}$ cm; a realistic value of h^A was selected as $h^A=1.68\times10^{-7}$ cm. With $\epsilon/\delta=8.75\times10^{-3}$, it results: $\alpha^A T/T_m^A=395.62$; $\alpha^B T/T_m^B=347.28$; $\tilde{\epsilon}^A=8.00\times10^{-4}$; $\tilde{\epsilon}^B=8.02\times10^{-4}$; $\tilde{W}^A=0.965$; $\tilde{W}^B=0.961$; $\tilde{L}=0.735$; $m=350$; $n=1.01$; $E=8\times10^{-3}$.

III. THE NUMERICAL METHOD

Equations (27) and (28) have been solved on a computational domain $-x_m\leqslant x\leqslant x_m$ with x_m large enough to prevent finite size effects. Neumann conditions were imposed at the domain's boundaries. Initially in the undercooled melt, at uniform temperature and concentration T and c^∞, a solid germ is nucleated at the center of the domain at $x=0$; the germ thickness is the minimum required to prevent remelting and to ensure the successive growth. The germ structural profile is obtained through a smooth tanh-like interpolation of the ϕ field between the values corresponding to the solid and liquid phases; the interface width is chosen as $\tilde{\epsilon}^A$, that is the nondimensional interface width of the pure solvent. The germ composition is assumed to be $c(0,0)=c^\infty$ when the melt temperature is $T<1702.5$ K; $c(0,0)$ is chosen on the solidus line for $T>1702.5$ K. An explicit Euler integration scheme was employed to advance the solution forward in time; second order central differences were used to discretize the Laplace operator. To ensure an accurate resolution of both the phase-field and concentration profiles, the grid spacing was selected as $\Delta x=0.5\tilde{\epsilon}^A$; a time step $\Delta t=0.4\times10^{-10}$ was required for numerical stability. To verify the consistency of the numerical scheme, at each time step the solute conservation was checked and in all the simulations was verified within 0.001%.

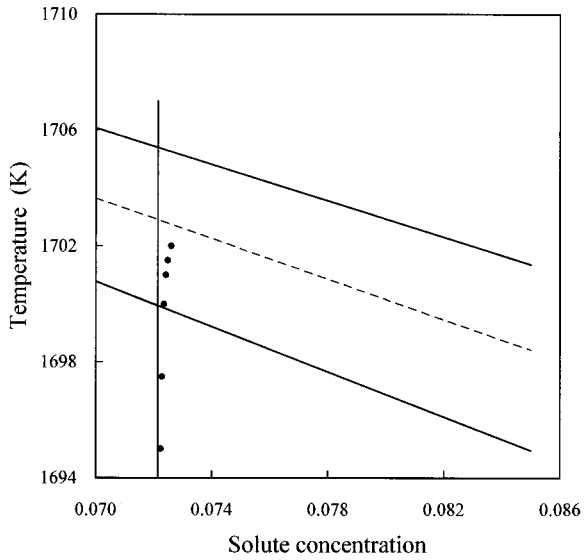

FIG. 1. A portion of the equilibrium phase diagram of the Ni-Cu alloy, computed from the data given in Table I. The vertical line corresponds to the value of c^∞ used in the simulations. The solid dots represent the pairs $(c_{\max},T)$ corresponding to the steady solutions found in the present study. From top to bottom, the corresponding steady velocities are, in nondimensional units, $v=2220$, $v=3600$, $v=4980$, $v=7725$, $v=14\,590$, $v=21\,455$. It is also indicated (dashed curve) the T_0 line.

IV. NUMERICAL RESULTS

The model presented above was proposed in a very similar version by WBM2, starting from a free-energy formulation; they developed an asymptotic analysis for $\epsilon/\delta\to0$ and solved in this limit the time independent equations. Equal solute diffusivities were assumed in the solid and liquid phases. As a result, given the far field concentration, and with temperature values below an upper limit, steady solutions were found for the interface velocity.

It is the aim of this section to study the growth process during its time evolution, until the solute profile is fully developed. At first, we present the results that correspond to the choice $D_s=0$. Excepting for temperatures, dimensionless units will be used throughout this section.

Figure 1 shows, in the (c,T) plane, the portion of the equilibrium phase diagram of the alloy that will be explored in the following. The initial concentration of the melt is set to $c^\infty=0.072\,14$, that belongs to the solidus line at $T=1699.8$ K. The solute segregation on the moving front is evaluated computing the maximum value $c_{\max}$ of $c(x,t)$, that identifies the concentration c_l on the liquid side of the interface. The solid dots superimposed on the graph represent the pairs $c_{\max}$, T corresponding to the steady long time solutions found in the numerical simulations. As expected, $c_{\max}$ increases with increasing the melt temperature, i.e., as the front velocity decreases. It is also indicated on the graph (dashed curve) the T_0 line, i.e., the locus of the pairs c, T for which the Helmholtz free energy of the liquid and solid are equal.

For $T\leqslant1702$ K after an initial transient the growth pro-

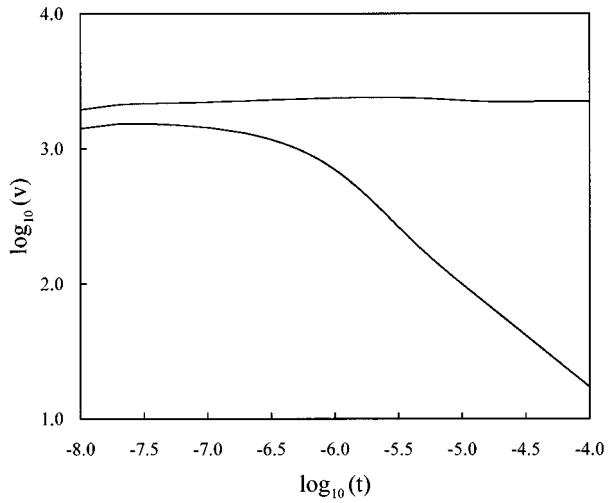

FIG. 2. Evolution of the front velocity with time for $T=1702$ K (upper curve) and $T=1704$ K (lower curve).

cess reaches steady state conditions, with the front velocity being a decreasing function of T; at $T=1704$ K it is clearly recognizable a long time evolution towards a diffusive regime, with the interface velocity decaying with time as $v \propto t^{-1/2}$. This behavior is shown in Fig. 2, where, for these two values of temperature, the interface velocity is represented versus time in a log-log plot.

Figure 3 shows the solute concentration profile at three different times; the system temperature is $T=1697.5$ K, a value that ensures long time steady growth. The steady solute boundary layer is developed along a transient time that is reflected in a distance of growth of about $x=0.035$; within this transient the liquid composition at the interface increases from c^{∞} to its steady value. Correspondingly, due to solute segregation, the interface solid composition c_s (which history can be reconstructed from the graph) falls from c^{∞} to a minimum at $x=0.008$, and reaches again c^{∞} at the steady state. The damped oscillation of the solute profile ahead of

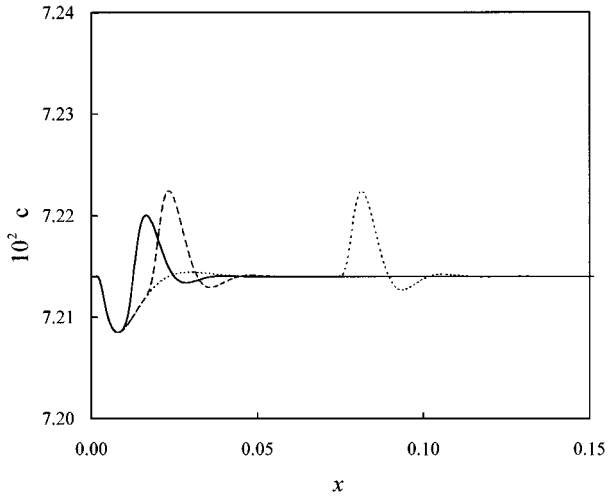

FIG. 3. Solute concentration profiles for $T=1697.5$ K, at three different times: $t=0.5\times10^{-6}$ (solid line), $t=1.0\times10^{-6}$, (dashed line) and $t=5.0\times10^{-6}$ (dotted line); time is given in nondimensional units.

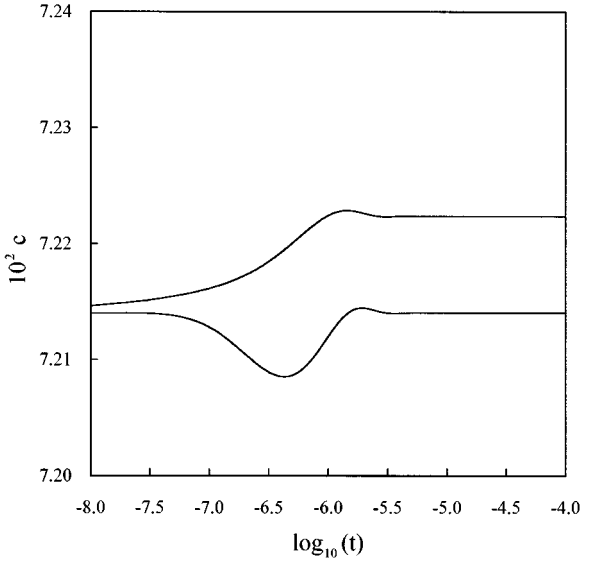

FIG. 4. Solute concentration on the solid side of the interface (lower curve) and on the liquid side of the interface (upper curve), versus time. $T=1697.5$ K.

the interface was predicted by WBM2 for sufficiently high growth velocity.

For the same value of temperature Fig. 4 shows c_s and c_l versus time. Solute segregation starts at the beginning of the growth process and a concentration gap is developed at the interface. The solid concentration falls to a minimum during the first stage of the growth, then c_s follows the increase of c_l until the steady value is reached. The liquid concentration evolves towards the steady value passing through a maximum at $t=1.46\times10^{-6}$; the duration of the transient is confined within $t\leqslant4\times10^{-6}$. The nonmonotonic evolution of c_l is probably due to the fourth order diffusion equation, and is not expected for the classical second order diffusion problem.

The continuous growth model of Aziz and Kaplan [4] gives the dependence of the partition coefficient on the growth velocity in the form

$$k(v)=\frac{k_e+v/v_d}{1+v/v_d}, \tag{32}$$

where v_d is a characteristic kinetic velocity for solute trapping, which is often taken as D/a, D being an interface diffusivity, and a the interatomic spacing. This result was substantially recovered by WBM2 for the long time steady solution of the phase-field model.

To extend the predictions of the CGM to the transient growth, Eq. (32) is solved for v_d fixing v and $k(v)$ at their steady values, found at $T=1697.5$ K. With $k_e=0.797$, it results $v_d=83.57$. Then the partition coefficient, as given by Eq. (32), is evaluated during the growth process, using the actual interface velocity. The result is compared in Fig. 5 with the actual ratio c_s/c_l found in the numerical simulation. The two curves indicate a strong difference in the time history of solute segregation as predicted by the two models; in front of the monotonic behavior of the CGM curve, the numerical simulation shows a partition coefficient that undergoes a damped oscillation before settling on its steady value.

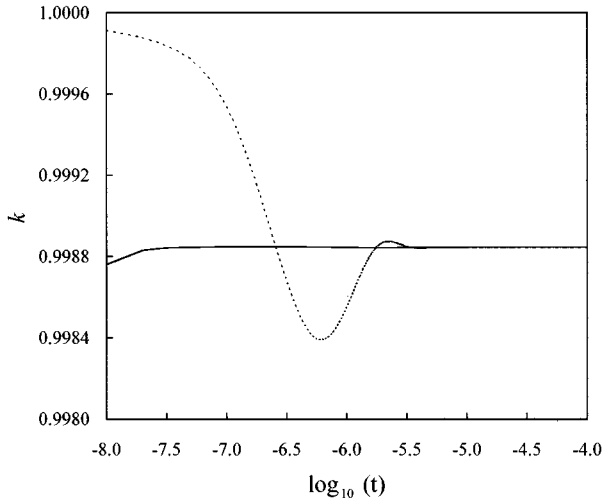

FIG. 5. Time evolution of the partition coefficient c_s/c_l as computed from the numerical simulation (dotted line) and from Eq. (32) (solid line). $T=1697.5$ K.

The value of c_s/c_l given by the numerical solution is very high in the first transient. It is worth noting that within the phase-field model the front velocity is finite at the startup of the process and the CGM [Eq. (32)] predicts an initial value of the partition coefficient $k(v)<1$. But the large c gradients that would result at the interface cannot be sustained, due to the high energy cost, and a transient time is required for the partition coefficient to relax on its steady value.

To the author's knowledge, at present no experimental data are available to suggest whether the CGM or the PFM gives a more realistic picture of the solute trapping in the early stage of the growth. The discrepancy of the two models is confined to a transient time of the order of 10^{-8} s and to a depth growth of the order of some hundreds of ångstroms. The experiments of Smith and Aziz [8] on aluminum alloys are the first performed on metallic systems; these authors

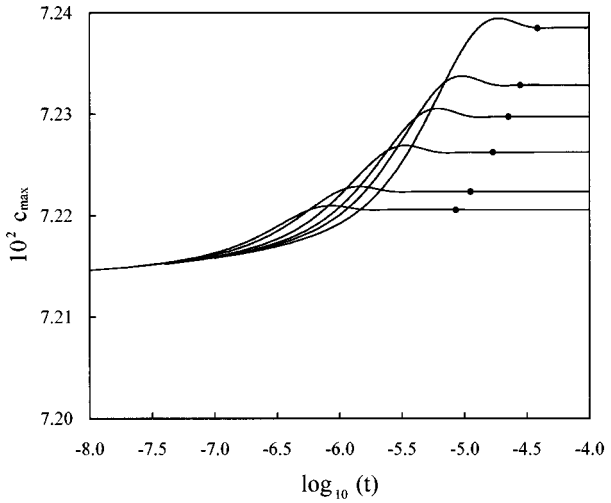

FIG. 6. Solute concentration on the liquid side of the interface, versus time. The curves correspond, from top to bottom, to $T=1702.0$ K, $T=1701.5$ K, $T=1701.0$ K, $T=1700.0$ K, $T=1697.5$ K, and $T=1695.0$ K. The solid dots superimposed on the curves mark the characteristic time of the transient stage t^*.

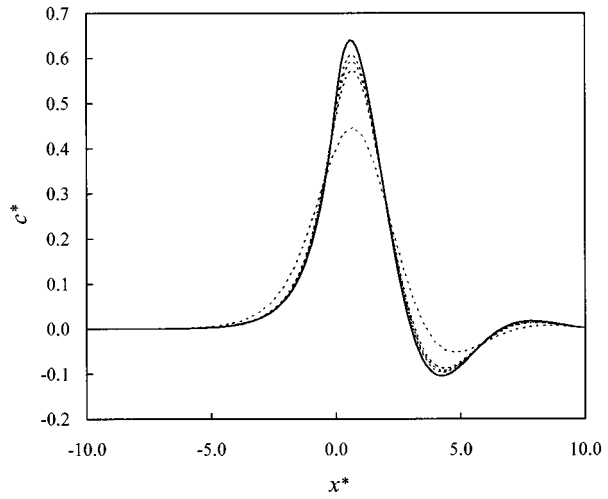

FIG. 7. A comparison of the computed concentration profiles for different values of E (dotted lines) with the asymptotic forms (33) and (34) (solid line). The computed curves correspond, in order of decreasing maxima, to $E=8\times10^{-3}$, $E=4\times10^{-3}$, $E=2\times10^{-3}$, and $E=0.2\times10^{-3}$. $D_s=D_l$; $T=1697.5$ K.

studied the rapid solidification of a doped aluminum film deposited on a silicon substrate; pulsed-laser melting was used to obtain growth velocities in the range 0.6–5.1 m/s. Unfortunately, due to experimental difficulties, the analysis of the solute profile discards just the first hundreds of ångstroms interested in the regrowth process.

The effect of the melt temperature on the solute peak at the interface is shown in Fig. 6, where $c_{\max}$ is represented versus time; the curves refer to different temperature values. The time required for $c_{\max}$ to reach the steady value depends on the melt temperature, i.e., on the growth rate. This result had to be expected; as pointed out by Wheeler, Boettinger, and Mcfadden [7], the solute profile contracts at large velocities and is described by the characteristic length $\ell^*=\xi\sqrt{E}[c^\infty(1-c^\infty)](v\sqrt{E})^{-1/3}$; then the time scale of the transient should be of the order of $t^*=\ell^{*2}/D_l$. This suggestion

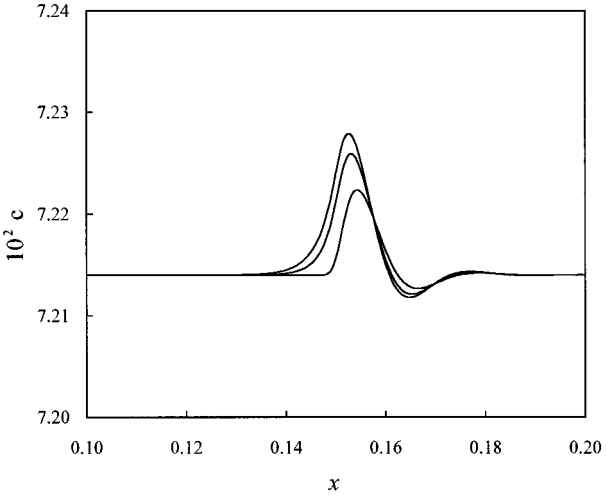

FIG. 8. Solute concentration profiles for different values of D_s/D_l; $T=1697.5$ K, $E=8\times10^{-3}$. The curves correspond (in order of increasing maxima) to $D_s/D_l=0$, 0.5, 1.

is confirmed observing the solid dots superimposed on the graph that indicate, for each curve, the corresponding value of t^*. The asymptotic analysis of WBM2 was performed for $D_s = D_l$, and in the limit $\epsilon/\delta \to 0$; in these conditions, and for sufficiently high growth velocities, the scaled concentration profile $c^* = (c - c^\infty)(v\sqrt{E})^{2/3}/\beta$ was shown to be a function of the scaled coordinate $x^* = (x/\sqrt{E})[v\sqrt{E}/c^\infty(1-c^\infty)]^{1/3}$ as

$$c^* = \exp\left(-\frac{x^*}{2}\right)\cos\left(\frac{x^*\sqrt{3}}{2} - \frac{\pi}{3}\right), \tag{33}$$

in the liquid ($x^* > 0$) and

$$c^* = \tfrac{1}{2}\,\exp(x^*) \tag{34}$$

in the solid ($x^* < 0$), where β is given by

$$\beta = \frac{2v_m[c^\infty(1-c^\infty)]^{2/3}}{3RT}\left[L^B\,\frac{T - T_m^B}{T_m^B} - L^A\,\frac{T - T_m^A}{T_m^A}\right]. \tag{35}$$

Figure 7 shows c^* versus x^* for $D_s = D_l$ and for different values of E, along with the curve given by Eqs. (33)–(35). The system temperature is $T = 1697.5$ K. It can be observed that the asymptotic solution is recovered to a quite good extent with $E = 8\times10^{-3}$, that corresponds to $\epsilon/\delta = 8.75\times10^{-3}$. It is worth noting that due to the scaling of c^*, the true solute peak at the interface decreases as the peak of c^* increases, so that the curves show that lower solute gradients are associated to higher values of the energy gradient coefficient for the solute field δ.

Figure 8 shows the influence of the ratio D_s/D_l on the steady solute profile, at $T = 1697.5$ K. The solute peak in the liquid is enhanced as the ratio D_s/D_l increases. This effect is in qualitative agreement with the predictions of the CGM: increasing the interface diffusivity causes a more effective solute-solvent redistribution across the interface resulting in a high kinetic velocity v_d and, through Eq. (32), in a high value of c_l.

V. CONCLUSIONS

The ability of the phase-field model to describe solute trapping during solidification was proved [7] for steady isothermal growth; in these conditions the phase-field predictions agree with the results of the continuous growth model. The present study extends the investigation to the early stage of the growth, when the solute profile is not yet fully developed. In this stage the phase-field model and the continuous growth model describe the solute segregation at the interface in a substantially different way.

The characteristic length of the solute profile $l^* = \xi\sqrt{E}[c^\infty(1-c^\infty)](v\sqrt{E})^{-1/3}$ suggests the time scale for the transient as $t^* = l^{*2}/D_l$. The numerical results confirm this prediction; in the range explored the transient relaxes within 10^{-8} s and is reflected in a growth depth of several hundreds of angstroms. In metallurgical applications these scales are of no relevance, and the two models agree for all practical purposes. However, the extent of the transient could have significant implications in pulsed-laser melting of thin doped films, conducted to remove ion implantation damages. In this case the prediction of the solute profile is strongly dependent on the model that is utilized. At present no experimental data are available to suggest whether the CGM or the PFM gives a more realistic picture of the solute trapping in the early stage of the growth. The diffusivity of the solid phase affects in a significant way the solute distribution across the interface; the ratio c_s/c_l decreases as D_s increases, confirming the suggestions of the CGM.

[1] Ch. Charach and B. Zaltzman, Phys. Rev. E **49**, 4322 (1994).
[2] Ch. Charach and Y. Keizman, in *Computational Modelling of Free and Moving Boundaries Problems*, edited by L. C. Wrobel, B. Sarler, and C. A. Brebbia (Computational Mechanics, Southampton, 1995).
[3] J. C. Baker and J. W. Cahn, Acta Metall. **17**, 575 (1969).
[4] M. J. Aziz and T. Kaplan, Acta Metall. **36**, 2335 (1988).
[5] M. J. Aziz and W. J. Boettinger, Acta Metall. **42**, 527 (1994).
[6] A. A. Wheeler, W. J. Boettinger, and G. B. McFadden, Phys. Rev. A **45**, 7424 (1992).
[7] A. A. Wheeler, W. J. Boettinger, and G. B. McFadden, Phys. Rev. E **47**, 1893 (1993).
[8] P. M. Smith and M. J. Aziz, Acta Metall. Mater. **42**, 3515 (1994).
[9] O. Penrose and P. C. Fife, Physica D **43**, 44 (1990).
[10] S. L. Wang, R. F. Sekerka, A. A. Wheeler, B. T. Murray, S. R. Coriell, R. J. Braun, and G. B. McFadden, Physica D **69**, 189 (1993).
[11] J. A. Warren and W. J. Boettinger, Acta Metall. Mater. **43**, 689 (1995).
[12] R. Willnecker, D. M. Herlach, and B. Feuerbacher, Phys. Rev. Lett. **62**, 2707 (1989).